This is a preprint, the final version is subject to change, of the American Mineralogist (MSA)
Cite as Authors (Year) Title. American Mineralogist, in press.
(DOI will not work until issue is live.) DOI: http://dx.doi.org/10.2138/am.2013.4202

H/D Isotope Effects in Brucite at Low-Temperatures

Bryan C. Chakoumakos[1], Juske Horita[2], Vasile O. Garlea[1]

[1] Quantum Condensed Matter Division
Oak Ridge National Laboratory, Oak Ridge, Tennessee 37831

[2] Department of Geosciences, Texas Tech University, Lubbock, Texas 79409

Abstract

Joint refinement of powder neutron diffraction data of hydrogenated and deuterated brucite over the temperature range of 10 – 295K clearly shows significant isotope effects in the structural parameters. $Mg(OH)_2$ has a 0.31% larger volume than that of $Mg(OD)_2$ at room temperature, which is mostly due to the *c*-axis expansion of $Mg(OH)_2$ as compared to $Mg(OD)_2$. The isotope affect in the *a*-axis has the opposite, but smaller, behavior as compared to the c-axis. These differences are slightly enhanced with reduction of the cell volume upon cooling. The temperature dependence of the isotropic atomic displacement parameters (ADPs) with the single site model show the ADP of the H atom is approximately larger than that of the D atom by the amount expected from the reduced-mass difference, but this difference is not evident with the split site model. Despite the shorter *c*-axis of the deuterated form, nearest-neighbor D…D distances are longer than the H…H distances, because the O-H distances are longer than the O-D distances, which necessarily places the H atoms closer together by 0.03 Å or more within the interlayer space. This study showcases an example of when a joint Rietveld refinement is ideally suited, by combining data for the deuterated and hydrogenated forms of brucite. The approach reduces the number of least-squares variables, and

reduces the systematic errors. It can be a general method to analyze isotope effects in materials studied by neutron diffraction.

Introduction

Brucite has been the subject of a number of parametric structural studies owing both to its importance as a building block of hydrous sheet silicates, particularly clay minerals, and as a model system for more complicated rock-forming minerals with both strong and weak chemical bonding. Both high pressure and variable temperature studies for brucite-type compounds have been made using diffraction (Catti et al. 1995; Chakoumakos et al. 1997; Desgranges et al. 1996; dos Santos et al. 2010; Fukui et al. 2003; Horita et al. 2010; Jayachandran and Liu 2006; Nagai et al. 2000a, 2000b; Parise et al. 1994; Shim et al. 2006; Xu et al. 2007a, 2007b), Brillouin scattering (Jiang et al. 2006), inelastic neutron scattering (Chakoumakos et al. 1997; Kazimirov et al. 2010), vibrational (Raman and infrared) spectroscopy (Shinoda et al. 2002; Shieh and Duffy 2002; Shim et al. 2006; Speziale et al. 2005), and a variety of theoretical modeling (Mitev et al. 2009; Azuma et al. 2011; Braterman and Cygan 2006; Hermansson et al. 2008, 2009; Civalleri et al. 2009; Jochym et al. 2010; Mookherjee and Stixrude 2006; Ulgliengo et al. 2009; Kirkpatrick et al. 2005; Reynard and Caracas 2009; Sainz-Diaz et al. 2000, Tosoni et al. 2005). We previously undertook a neutron powder diffraction study of the H/D effect in brucite as a function of pressure (Horita et al. 2010). Here we report an ambient pressure study of the same effect as a function of temperature using higher resolution data. The present work corroborates the previous findings and gives a more detailed view of the isotope effect and thermal contraction mechanism in brucite.

Experimental Methods

After removing fines by elutriation in water, MgO powder (99.95% purity on metal basis, Alfa Aesar) was heated in vacuum at 900° C for 2 days to remove traces of water. The dehydrated MgO (10 g) was loaded into a Teflon cup along with 80 g of either de-ionized water (D/H ~ 0.015%) or heavy water (99.9% purity, Cambridge Isotope Laboratory), then sealed inside a 300 mL reaction vessel, and heated to 300° C (ca. 8.5 MPa vapor-saturated pressure) for 2 weeks to hydrothermally synthesize the hydrogenated or deuterated brucite. Previous X-ray and neutron powder diffraction and Raman spectroscopy confirmed the product of these reactions to be pure brucite with greater >99% of deuteration for the $Mg(OD)_2$ sample (Horita et al. 2010).

Neutron powder diffraction measurements were performed at the HB-2A high resolution powder diffractometer located at the High Flux Isotope Reactor at Oak Ridge National Laboratory (Garlea et al. 2010). Powdered samples were loaded in vanadium cans and placed in a top loading low temperature cryostat. The wavelength of 1.1176 Å produced by a Ge [115] monochromator was used and Soller collimation of 12', 21', 6', before the monochromator, before the sample, and before the detectors, respectively. For each sample a data set over the 2θ range 10 – 132° was collected with a step size of ~ 0.067°, counting 60s per step, at the temperatures 20, 30, 40, 50, 60, 70, 80, 90, 100, 120, 150, 200, and 295 K.

Rietveld refinements were made using the FullProf suite (Rodriguez-Carvajal 1993). Scattering lengths used were 5.375, 5.803, 6.671, -3.739 fm for Mg, O, D, and H, respectively. To reduce the number of least squares variables and increase the amount of

data, a combined refinement using both neutron datasets of the hydrogenated and deuterated samples was undertaken. This approach also should lessen the effects of any systematic errors. The resolution of these data was much higher than those from our previous high pressure study on H/D effects in brucite (Horita et al. 2010). Previous studies have employed anisotropic, split-site, or anharmonic to account for the large displacements of the H/D atom (Desgranges et al. 1993, 1996; Parise et al. 1994; Chakoumakos et al. 1997). Here, we have used a split-site model for the H/D atom position.

Brucite has space group symmetry $P\text{-}3m1$, with atomic positions: Mg 0,0,0 ; O $\frac{1}{3},\frac{2}{3},z$; and D/H $\frac{1}{3},\frac{2}{3},z$ for the single site model and $\frac{1}{3},y,z$ for the split-site model. Parameters refined in common included the peak shapes and the Mg and O isotropic atomic displacement parameters. Parameters refined for each dataset included lattice parameters; O, D, or H atom y and z coordinates; D or H isotropic atomic displacement parameters; diffractometer zero; preferred orientation, scale factor; and background. The peak shape function used was the Thompson-Cox-Hastings pseudo-Voigt function with axial divergence asymmetry. Asymmetry parameters S/L and D/L were fixed at 0.034 and 0.035 respectively, and two additional peak asymmetry parameters were refined. The backgrounds were defined by 3rd order and 8th order polynomials with their origin at 60° 2θ, for the deuterated and hydrogenated data, respectively. The displacements of all atoms were refined isotropically. The deuterium content of the deuterated sample was fixed at unity, based on previous Raman spectroscopy and neutron diffraction analysis. Both single-site and split-site models for the H/D position were made and compared.

Results

Typical neutron powder diffraction patterns are shown for hydrogenated and deuterated brucite in Figure 1. The principal difference between the two patterns, other than the different intensities due to the different scattering factors of the D and H atoms, is the much larger background of the hydrogenated sample due to the nuclear spin incoherent scattering contribution from the H atoms.

The temperature dependence of the lattice parameters over the range 20 – 295K shows Debye behavior (Fig. 2). The *c*-axis is smaller for the deuterated brucite as compared to the hydrogenated brucite for all temperatures and this difference increases slightly upon cooling, Δc(295K) = 0.015 Å, Δc(20K) = 0.02 Å. The *a*-axis shows the opposite behavior, but the difference is more than an order of magnitude smaller, Δa(295K) = -0.001 Å, Δa(20K) = -0.0005 Å. The net result is that the volume of the deuterated brucite is smaller than that of the hydrogenated brucite at 295K by 0.15 $Å^3$, or 0.31%, which compares well with the room temperature difference, 0.34%, determined by X-ray diffraction (Horita et al. 2010).

The temperature dependence of the isotropic atomic displacement parameters (ADP) exhibits the expected variation (Fig. 3), except that the values for the oxygen atom are lower than those for the magnesium atom. The ADP of the H atom is larger than that of the D atom by approximately the amount expected from the difference in their reduced masses ($\frac{1x16}{1+16}$ and $\frac{2x16}{2+16}$ for O-H and O-D, respectively) within a harmonic oscillator model. For the split-site model, the ADP's of H and D coincidentally collapse to common values (Fig. 3b).

The O-D, O-H, and MgO bond lengths of deuterated and hydrogenated brucite show essentially little or no temperature dependence (Fig. 4 and 5). This follows from the lack of any significant temperature dependence of the *z*-coordinates of the O, D, and H atom positions (Fig. 6). The refined values of the z-coordinates of the O and H atoms for the hydrogenated brucite show a clear model dependence, which gives rise to model dependent Mg-O distance (Fig. 5). The room temperature value of the *z*(D) is smaller indicating a small increase in *z*(D) upon cooling from room temperature to ~100K. The *z*(O) of $Mg(OD)_2$ also show a small increase with decreasing temperature. Although, the *z*(O) was refined independently for each of the hydrogenated and deuterated data sets, the resulting same values indicate that this parameter could have also been held in common for the joint refinement. At 295K the O-D bond length is 0.965 Å as compared to the O-H bond length of 1.025 Å. The O-D distance compares favorable with the average value of 0.95 Å for 131 O-D bonds in the Inorganic Crystal structure Database (ICSD) determined by single-crystal neutron diffraction. The ICSD values are uncorrected for thermal motion, so an additional shortening of ~0.01- 0.02 Å is expected. It is known generally that O-D distances are shorter than O-H distances, including liquid water: O-H, 0.991 and O-D, 0.970 Å (Ichikawa et al. 1991; Silvestrelli and Parrinello 1999).

The nearest-neighbor H…H distances are essentially constant within error over the temperature range 20K – 300K (Fig. 7). In contrast, the D…D distances show a systematic shortening upon cooling and plateau below 100K. Overall the D…D distances are longer than the H…H distances by 0.03 Å or more. This might seem counter-intuitive given that the volume of the deuterated brucite is smaller than the hydrogenated brucite, but the O-H distances are longer than the O-D distances so the

H…H distances are necessarily closer within the interlayer space. In addition, a small contribution also comes from the a-axis of the deuterated brucite being slightly longer than that of hydrogenated brucite.

The temperature dependence of the splitting of the H/D site basically follows the same behavior as the atomic displacement parameters (see Fig. 3). The magnitude of the splitting is larger for the H site as compared to the D site because the H atomic displacement is larger, and the splitting decreases with temperature because the thermal vibration decreases.

Temperature dependence of the octahedral layer thickness and the interlayer thickness in deuterated brucite shows that the octahedral layer thickness remains constant, whereas the interlayer thickness contraction accommodates the observed *c*-axis contraction (Fig. 8). This behavior is expected given the weak Van der Waals interaction between the layers, but is opposite to that reported by Chakoumakos et al. (1997) from an analysis of t-o-f neutron diffraction data. It is evident that the previous study by Chakoumakos et al. (1997) on the low temperature behavior of deuterated brucite using t-of-f neutron diffraction data has some systematic errors in the refinement of the atomic positions. Even though the data used here does not extend to as high resolution, the temperature dependence of the structural changes is more crystal chemically sensible.

Discussion

This study showcases an example of when a joint Rietveld refinement is ideally suited, by combining data for the deuterated and hydrogenated forms of brucite. The approach reduces the number of least-squares variables, and reduces the systematic

errors. It can be a general method to analyze isotope effects in materials studied by neutron diffraction. The D/H isotope effect on the lattice parameters of brucite is easily measured by either neutron or X-ray diffraction, but structural details beyond the lattice dimensions require the use of neutron diffraction.

The model dependence, albeit small, of the refined *z*-coordinates for the H and O positions for the hydrogenated brucite is disconcerting (Fig. 6). The origin of this systematic error may stem from the overall lower peak intensities (i.e., higher background) and/or a poorer modeling of the larger ADP of the H atom. Nevertheless, we give more credibility to the split-site model which overall offers slightly better fits to the data for each temperature. The refinements for the deuterated brucite give the same results for both the single-site and split-site models. That the splitting does not reduce to zero at zero temperature, reinforces the view that the H/D atom is positional disordered and does not in fact reside on the 3-fold axis.

That the differences in the unit cell dimensions between deuterated and hydrogenated brucite increase with reducing cell volume as show here are consistent with our previous finding that the isotope effect increases with pressure. Our results show that the volume contraction at 20-295 K corresponds to that of pressure increase to ca. 0.4 GPa at room temperature (Horita et al. 2010). In essence, the lower zero-point energy of deuterium implies a smaller vibration amplitude, hence smaller molecular or unit-cell size, than that of hydrogen. A quantized harmonic oscillator model suggests that the zero-point motion is inversely proportional to the square-root of the reduced mass, and hence smaller for the deuterated compounds. However, the effect of temperature is opposite, to expand the effective size of deuterium faster than that of hydrogen. Thus, for

a system with low-frequency vibrations, deuterated compounds may even become larger than their hydrogenated counterparts at sufficiently high temperatures (Dunitz et al. 2008). This study at low temperature and our previous study at elevated pressures (Horita 2010) together show that in case of brucite (and likely other hydrous minerals), deuterated minerals have smaller unit-cell volume, probably in the entire P-T space. This measured effect of H–D substitution on the unit-cell volume demonstrates that brucite (and other hydrous minerals) preferentially incorporate deuterium over hydrogen under pressure (Horita et al. 2010), with the implications that the distribution of hydrogen isotopes in deep-earth conditions may differ significantly from that in near-surface environments.

Several studies suggested that high-pressure compression accentuates proton disorder in brucite. As the octahedral layers are compressed along the *c* axis, the interlayer and O…H(D) distances become shorter, while the intralayer O-H(D) bond length stays nearly constant or shortens only slightly. Then, hydrogen atoms of two O-H(D) groups from adjacent octahedral layers may start to repulse (H-H repulsion), causing such structural changes. However, two high-pressure neutron diffraction studies, using hydrogenated and deuterated brucite (Catti et al. 1995; Parise et al. 1994) provided somewhat contradicting results. Our study of the two brucites here clearly demonstrate differences in O-H(D) and H(D)…H(D) parameters during thermal contraction. If the changes observed in these parameters upon cooling are similar to those under pressure, an implication from the high-pressure neutron diffraction studies cannot be substantiated, namely D…D repulsion is stronger than H…H repulsion, because the D…D distance is greater than H…H (Fig. 7). To test this hypothesis, a companion high-resolution neutron

diffraction study is needed of $Mg(OH)_2$ and $Mg(OD)_2$ with a joint Rietveld refinement. This and our previous study (Horita et al., 2010) clearly demonstrate that caution must be exercised in using deuterated compounds for neutron scattering experiment to avoid incoherent scattering from hydrogen.

Acknowledgments

Research at Oak Ridge National Laboratory's High Flux Isotope Reactor was sponsored by the Scientific User Facilities Division, Office of Basic Energy Sciences, U. S. Department of Energy.

References Cited

Azuma, K., Oda, T., and Tanaka, S. (2011) Vibration analysis of O-H stretching mode in $Mg(OH)_2$, $Ca(OH)_2$, LiOH, and NaOH by plane-wave pseudopotential DFT calculation. Computational and Theoretical Chemistry, 963, 215-220.

Braterman, P. S. and Cygan, R.T. (2006) Vibrational spectroscopy of brucite: A molecular simulation investigation. American Mineralogist, 91, 1188-1196.

Catti, M., Ferraris, G., Hull, S., and Pavese, A. (1995) Static Compression and H-Disorder in Brucite, $Mg(OH)_2$, to 11 GPa - a Powder Neutron-Diffraction Study. Physics and Chemistry of Minerals 22(3):200-206

Chakoumakos, B.C., Loong, C.K., and Schultz, A.J. (1997) Low-temperature structure and dynamics of brucite. Journal of Physical Chemistry B, 101, 9458-9462.

Civalleri, B., Ugliengo, P., Zicovich-Wilson, C.M., and Dovesi, R. (2009) Ab initio modeling of layered materials with the CRYSTAL code: an overview. Zeitschrift für Kristallographie, 224, 241-250.

Desgranges, L., Grebille, D., Galvarin, G., Chevrier, G., Floquet, N., and Niepce, J.-C. (1993) Hydrogen thermal motion in calcium hydroxide - $Ca(OH)_2$. Acta Crystallographica, B49, 812-817.

Desgranges, L., Galvarin, G., and Chevrier, G. (1996) Interlayer interactions in $M(OH)_2$: A neutron diffraction study of $Mg(OH)_2$. Acta Crystallographica, B52, 82-86.

dos Santos, A. M., Horita, J., Tulk, C. A., Chakoumakos, B. C., Polyakov, V. B. (2010) Combined high-pressure neutron and X-ray diffraction study of H-D substitution effects on brucite. Geochimica et Cosmochimica Acta, 74, A244-A244, Supplement 1.

Dunitz, J.D. and Ibberson, R.M. (2008) Is deuterium always smaller than protium? Angewandte Chemie International Edition 47, 4208-4210.

Evans, D.G. and Slade, R.C.T. (2006) Structural aspects of layered double hydroxides. In Editors: Duan X. and Evans D. G., Layered Double Hydroxides. Structure and Bonding, 119, 1-87.

Fukui, H., Ohtaka, O., Suzuki, T., and Funakoshi, K. (2003) Thermal expansion of $Mg(OH)_2$ brucite under high pressure and pressure dependence of entropy. Physics and Chemistry of Minerals, 30, 511-516.

Garlea, V. O., Chakoumakos, B. C., Moore, S. A., Taylor, G. B., Chae, T., Maples, R. G., Riedel, R. A., Lynn, G. W., and Selby, D. L. (2010) The high-resolution powder diffractometer at the High Flux Isotope Reactor. Applied Physics A-Materials Science & Processing, 99, 531-535.

Hermansson, K., Probst, M.M., Gajewski, G., and Mitev, P.D. (2009) Anharmonic OH vibrations in $Mg(OH)_2$ (brucite): Two-dimensional calculations and crystal-induced blueshift. Journal of Chemical Physics, 131, 244517.

Hermansson, K., Gajewski, G., and Mitev, P. D. (2008) Pressure-induced OH frequency downshift in Brucite: frequency-distance and frequency-field correlations. In Editors: Dovesi, R., Orlando, R., and Roetti C, Ab initio simulation of crystalline solids: history and prospects - contributions in honor of Cesare Pisani. Journal of Physics Conference Series, 117, 12018-12018.

Horita, J., dos Santos, A. M., Tulk, C. A., Chakoumakos, B. C., and Polyakov, V. B. (2010) High-pressure neutron diffraction study on H-D isotope effects in brucite. Physics and Chemistry of Minerals, 37, 741-749.

Ichikawa, K., Kameda, Y., Yamaguchi, T., Wakita, H. and Misawa, M., Neutron-diffraction investigation of the intramolecular structure of a water molecule in the liquid-phase at high-temperatures, Molecular Physics 73 (1991) 79-86.

Jayachandran, K.P. and Liu, L.G. (2006) High pressure elasticity and phase transformation in brucite, $Mg(OH)_2$. Physics and Chemistry of Minerals, 33, 484-489.

Jiang, F.M., Speziale, S., and Duffy, T.S. (2006) Single-crystal elasticity of brucite, $Mg(OH)_2$, to 15 GPa by Brillouin scattering. American Mineralogist, 91, 1893-1900.

Jochym, P.T., Oles, A.M., Parlinski, K., Lazewski, J., Piekarz, P., and Sternik, M. (2010) Structure and elastic properties of $Mg(OH)_2$ from density functional theory. Journal of Physics-Condensed Matter, 22, 445403.

Kazimirov, V. Yu., Smirnov, M. B., Bourgeois, L., Guerlou-Demourgues, L., Servant, L., Balagurov, A. M., Natkaniec, I., Khasanova, N. R., and Antipov, E.V. (2010) Atomic structure and lattice dynamics of Ni and Mg hydroxides. Solid State Ionics, 181, 1764-1770.

Kirkpatrick, R.J., Kalinichev, A.G., and Wang, J. (2005) Molecular dynamics modeling of hydrated mineral interlayers and surfaces: structure and dynamics. Mineralogical Magazine, 69, 289-308.

Mitev, P.D., Gajewski, G., and Hermansson, K. (2009) Anharmonic OH vibrations in brucite: Small pressure-induced redshift in the range 0-22 GPa. American Mineralogist, 94, 1687-1697.

Mookherjee, M. and Stixrude, L. (2006) High-pressure proton disorder in brucite. American Mineralogist, 91, 127-134.

Nagai, T., Ito, T., Hattori, T., and Yamanaka, T. (2000a) Compression mechanism and amorphization of portlandite, $Ca(OH)_2$: structural refinement under pressure. Physics and Chemistry of Minerals, 27, 462-466.

Nagai, T., Hattori, T., and Yamanaka, T. (2000b) Compression mechanism of brucite: An investigation by structural refinement under pressure. American Mineralogist, 85, 760-764.

Parise, J. B., Leinenweber, K., Weidner, D. J., Tan, K., and Von Dreele, R. B., (1994) Pressure-induced H-bonding - neutron-diffraction study of brucite, $Mg(OD)_2$, to 9.3 GPa. American Mineralogist, 79, 193-196.

Reynard, B. and Caracas, R. (2009) D/H isotopic fractionation between brucite $Mg(OH)_2$ and water from first-principles vibrational modeling. Chemical Geology, 262, 159-168.

Rodriguez-Carvajal, J. (1993) Recent advances in magnetic-structure determination by neutron powder diffraction. Physica B 192, 55–69.

Sainz-Diaz, C.I. Timon, V., Botella, V., and Hernandez-Laguna, A. (2000) Isomorphous substitution effect on the vibration frequencies of hydroxyl groups in molecular cluster models of the clay octahedral sheet. American Mineralogist, 85, 1038-1045.

Shieh S.R. and Duffy, T.S. (2002) Raman spectroscopy of $Co(OH)_2$ at high pressures: Implications for amorphization and hydrogen repulsion. Physical Review B, 66, 134301.

Shim, S. -H., Rekhi, S., Martin, M. C., and Jeanloz, R. (2006) Vibrational spectroscopy and X-ray diffraction of $Cd(OH)_2$ to 28 GPa at 300 K. Physical Review B, 74, 024107.

Shinoda, K., Yamakata, M., Nanba, T., Kimura, H., Moriwaki, T., Kondo, Y., Kawamoto, T., Niimi, N., Miyoshi, N., and Aikawa, N. (2002) High-pressure phase

transition and behavior of protons in brucite $Mg(OH)_2$: a high-pressure-temperature study using IR synchrotron radiation. Physics and Chemistry of Minerals, 29, 396-402.

Silvestrelli, P. L. and Parrinello, M. (1999) Structural, electronic, and bonding properties of liquid water from first principles. Journal of Chemical Physics, 111, 3572-3580.

Speziale, S., Jeanloz, R., Milner, A., Pasternak, M.P., and Zaug, J.M. (2005) Vibrational spectroscopy of $Fe(OH)_2$ at high pressure: Behavior of the O-H bond. Physical Review B, 71, 184106.

Tosoni, S., Pascale, F., Ugliengo, P., Orlando, R., Saunders, V.R., and Dovesi, R. (2005) Quantum mechanical calculation of the OH vibrational frequency in crystalline solids. Molecular Physics, 103, 2549-2558.

Ugliengo, P., Zicovich-Wilson, C.M., Tosoni, S., and Civalleri, B. (2009) Role of dispersive interactions in layered materials: a periodic B3LYP and B3LYP-D* study of $Mg(OH)_2$, $Ca(OH)_2$ and kaolinite. Journal of Materials Chemistry, 19, 2564-2572.

Wang, J.W., Kalinichev, A.G., and Kirkpatrick, R.J. (2004) Molecular modeling of water structure in nano-pores between brucite (001) surfaces. Geochimica et Cosmochimica Acta, 68, 3351-3365.

Xu, H., Zhao, Y., Vogel, S. C., Daemen, L. L., and Hickmott, D. D. (2007a) Anisotropic thermal expansion and hydrogen bonding behavior of portlandite: A high-temperature neutron diffraction study. Journal of Solid State Chemistry, 180, 1519-1525.

Xu, H.W., Zhao, Y.S., Zhang, J.Z., Hickmott, D.D., and Daemen, L.L. (2007b) In situ neutron diffraction study of deuterated portlandite $Ca(OD)_2$ at high pressure and temperature. Physics and Chemistry of Minerals, 34, 223-232.

Figure Captions

Figure 1. Typical Rietveld refinement fits for hydrogenated (top) and deuterated (bottom) brucite using 1.1176 Å neutrons.

Figure 2. Temperature dependence of the lattice parameters and the unit cell volume of $Mg(OD)_2$ and $Mg(OH)_2$. $Mg(OH)_2$ has a 0.31% larger volume than that of $Mg(OD)_2$ at room temperature, which is mostly due to the *c*-axis expansion of $Mg(OH)_2$ as compared to $Mg(OD)_2$. The isotope effect in the a-axis is opposite, but smaller, than that in the *c*-axis.

Figure 3. Temperature dependence of the isotropic atomic displacement parameters (ADPs) from joint refinement of $Mg(OD)_2$ and $Mg(OH)_2$. (left) Single-site model shows larger displacements of H as compared to D due to the mass difference. (right) Split-site model results in H/D displacements collapsed to common values.

Figure 4. Temperature dependence of the O-D and O-H bond lengths of $Mg(OD)_2$ and $Mg(OH)_2$. Both the single site and split site models yield same values within the standard uncertainties. The distances have been corrected for the large thermal motion of the D and H atoms by $d(XO)_{corrected} = d(XO) + (U_x - U_o)/d(XO)$, where *U*'s are the displacements normal to the bond and X = H or D.

Figure 5. Temperature dependence of the Mg-O bond length of $Mg(OD)_2$ and $Mg(OH)_2$. Little change is observed over this temperature range, and larger errors and scatter are observed for $Mg(OH)_2$. For $Mg(OH)_2$ the Mg-O distance is model dependent.

Figure 6. Comparison of the temperature dependence of the *z*-coordinates of the O atom (top) and the D or H atom (bottom) in $Mg(OD)_2$ and $Mg(OH)_2$, where again the $Mg(OH)_2$ values are model dependent.

Figure 7. (top) Temperature dependence of the nearest-neighbor D…D and H…H distances in $Mg(OD)_2$ and $Mg(OH)_2$ for the single-site model. (bottom) Temperature dependence of the H/D site splitting as modeled with isotropic atom displacement parameters.

Figure 8. Temperature dependence of the octahedral layer thickness and the interlayer thickness in $Mg(OD)_2$. The octahedral layer thickness remains constant, whereas the interlayer thickness contraction accommodates the observed *c*-axis contraction. This behavior is expected given the weak interaction between the layers, but is opposite to that reported by Chakoumakos et al. (1997) from an analysis of t-o-f neutron diffraction data.

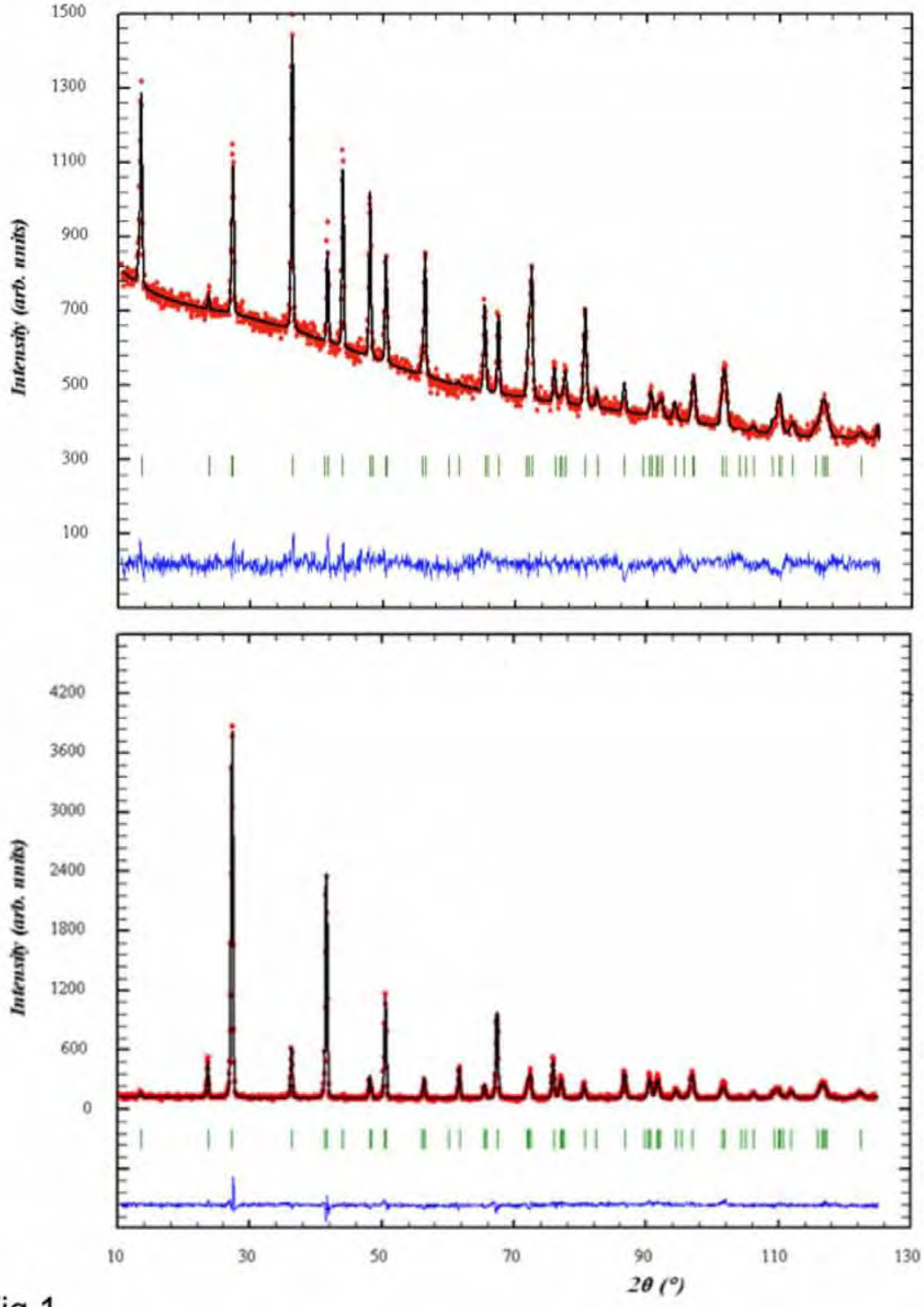
1500
1300
1100
900
700
500
300
100
Intensity (arb. units)
4200
3600
3000
2400
1800
1200
600
0
Intensity (arb. units)
10
30
50
70
90
110
130
2θ (°)

Fig 1

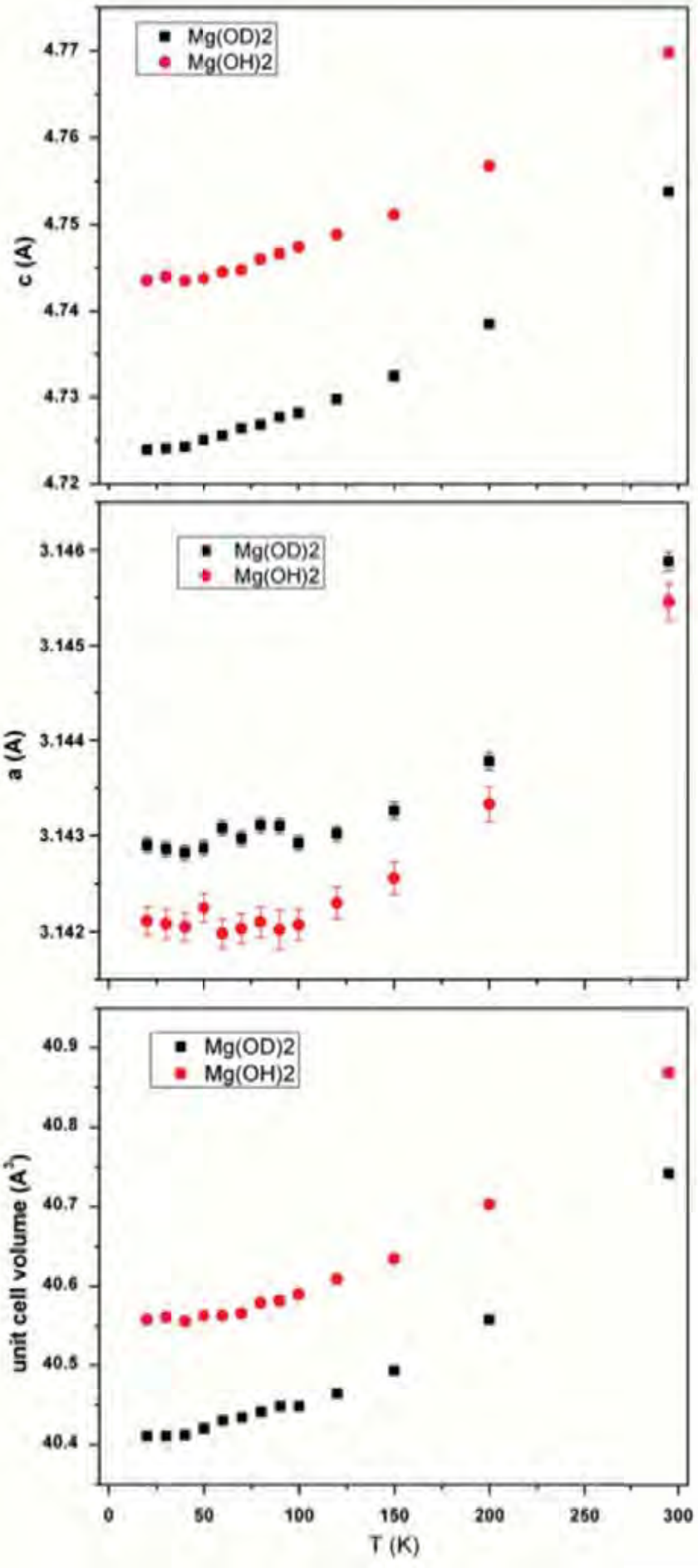
Mg(OD)2
Mg(OH)2
c (A)
4.77
4.76
4.75
4.74
4.73
4.72
Mg(OD)2
Mg(OH)2
a (A)
3.146
3.145
3.144
3.143
3.142
Mg(OD)2
Mg(OH)2
unit cell volume (A^3)
40.9
40.8
40.7
40.6
40.5
40.4
0
50
100
150
200
250
300
T (K)

Fig 2

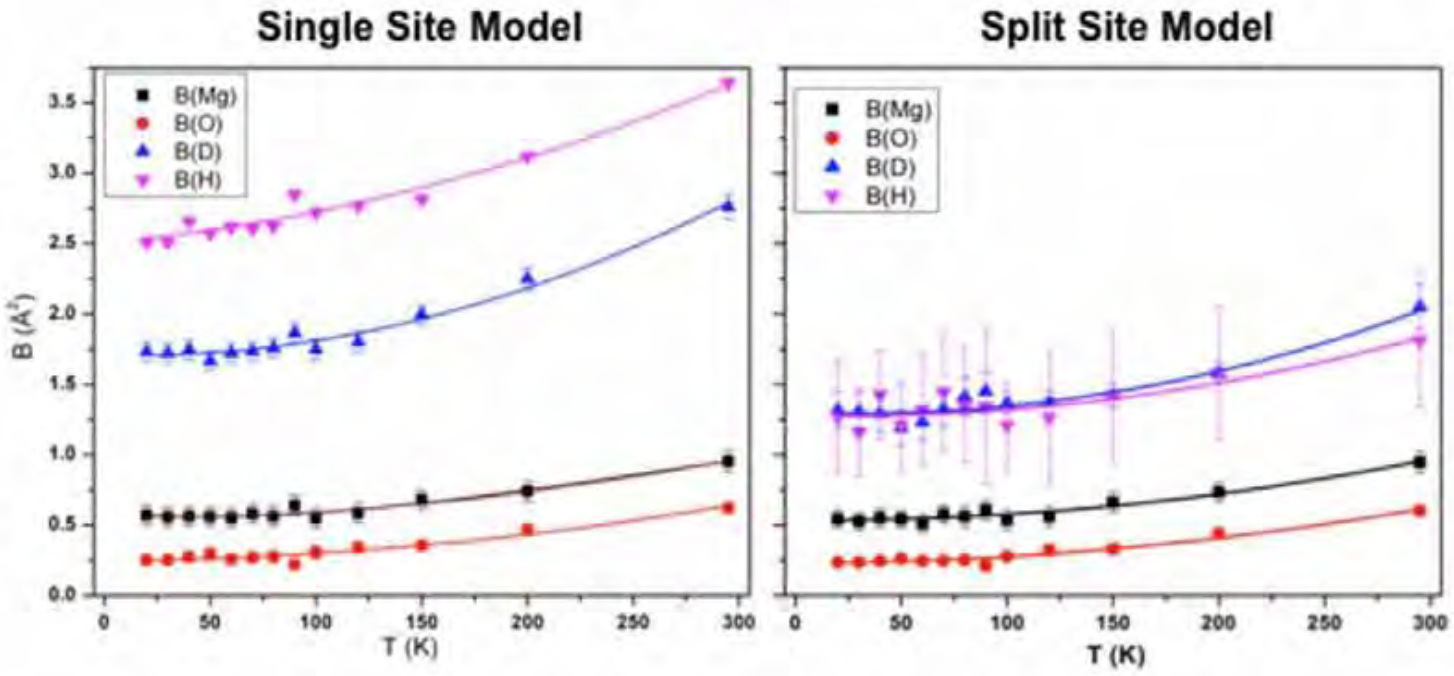
Single Site Model
Split Site Model
B(Mg)
B(O)
B(D)
B(H)
B (Å²)
T (K)
0.0
0.5
1.0
1.5
2.0
2.5
3.0
3.5
0
50
100
150
200
250
300

Fig 3

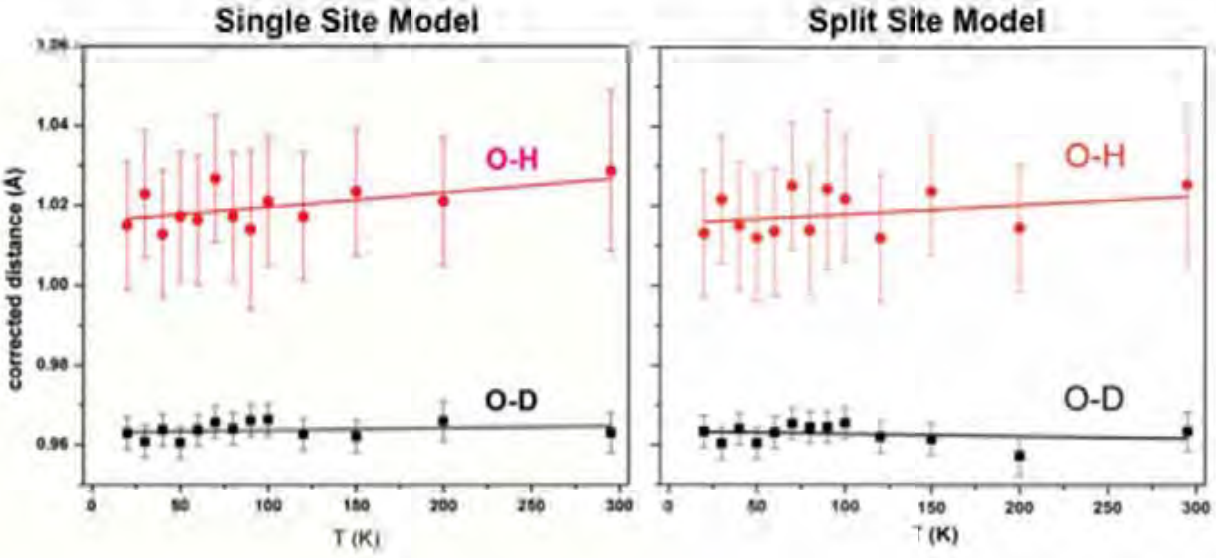
Single Site Model
Split Site Model
corrected distance (Å)
1.04
1.02
1.00
0.98
0.96
O-H
O-D
0
50
100
150
200
250
300
T (K)

Fig 4

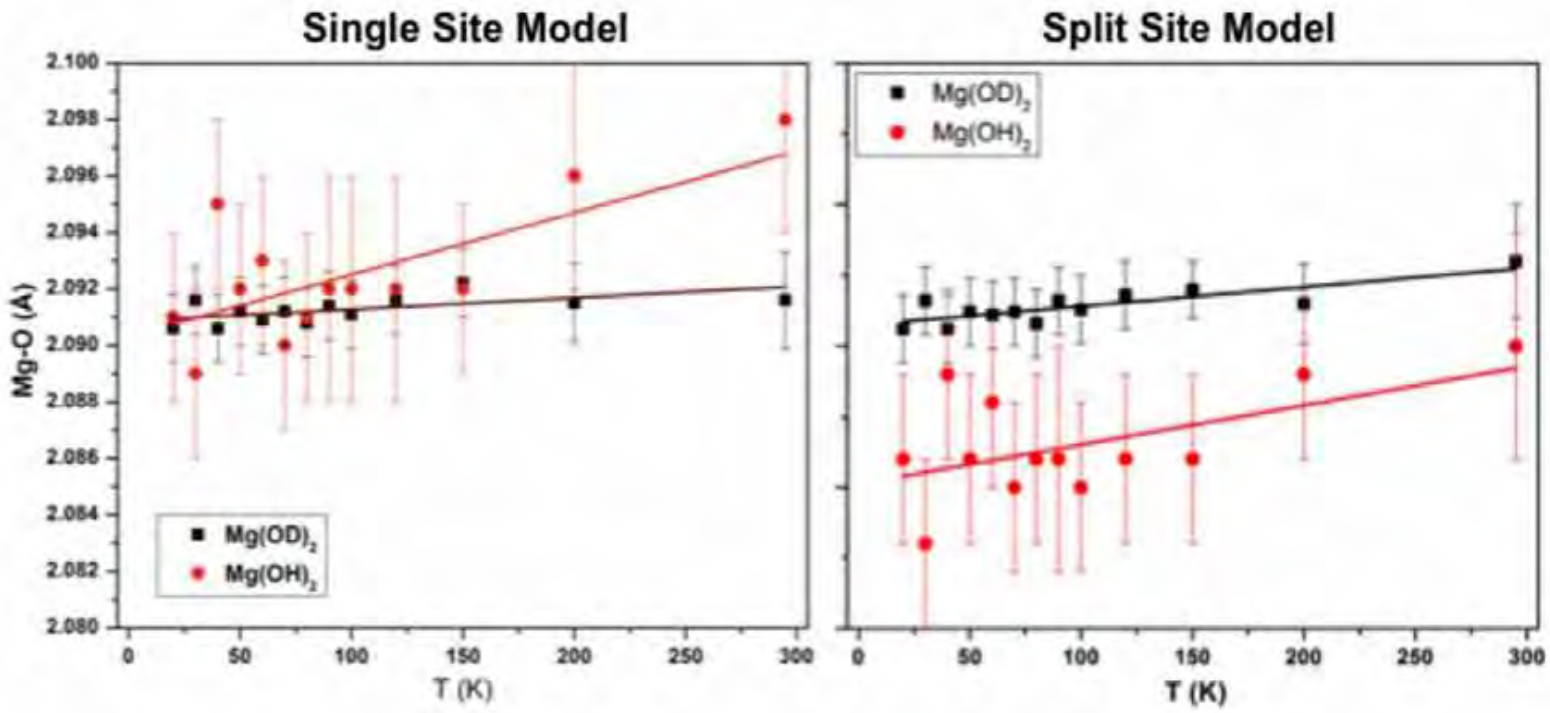
Single Site Model
Split Site Model
Mg-O (Å)
2.100
2.098
2.096
2.094
2.092
2.090
2.088
2.086
2.084
2.082
2.080
Mg(OD)2
Mg(OH)2
0
50
100
150
200
250
300
T (K)

Fig 5

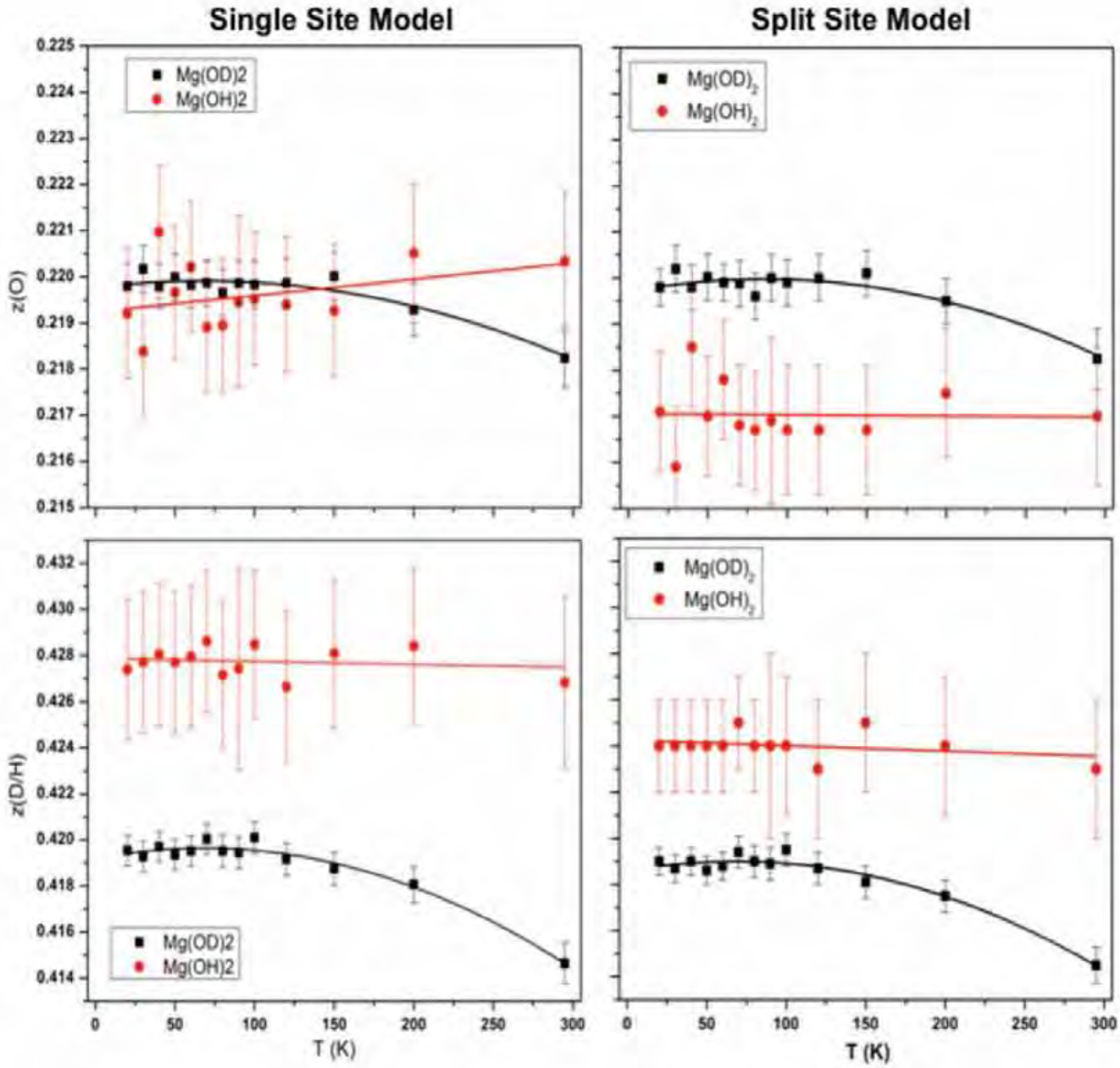
Single Site Model
Split Site Model
Mg(OD)2
Mg(OH)2
Mg(OD)$_2$
Mg(OH)$_2$
z(O)
z(D/H)
T (K)
0.225
0.224
0.223
0.222
0.221
0.220
0.219
0.218
0.217
0.216
0.215
0.432
0.430
0.428
0.426
0.424
0.422
0.420
0.418
0.416
0.414
0
50
100
150
200
250
300

Fig 6

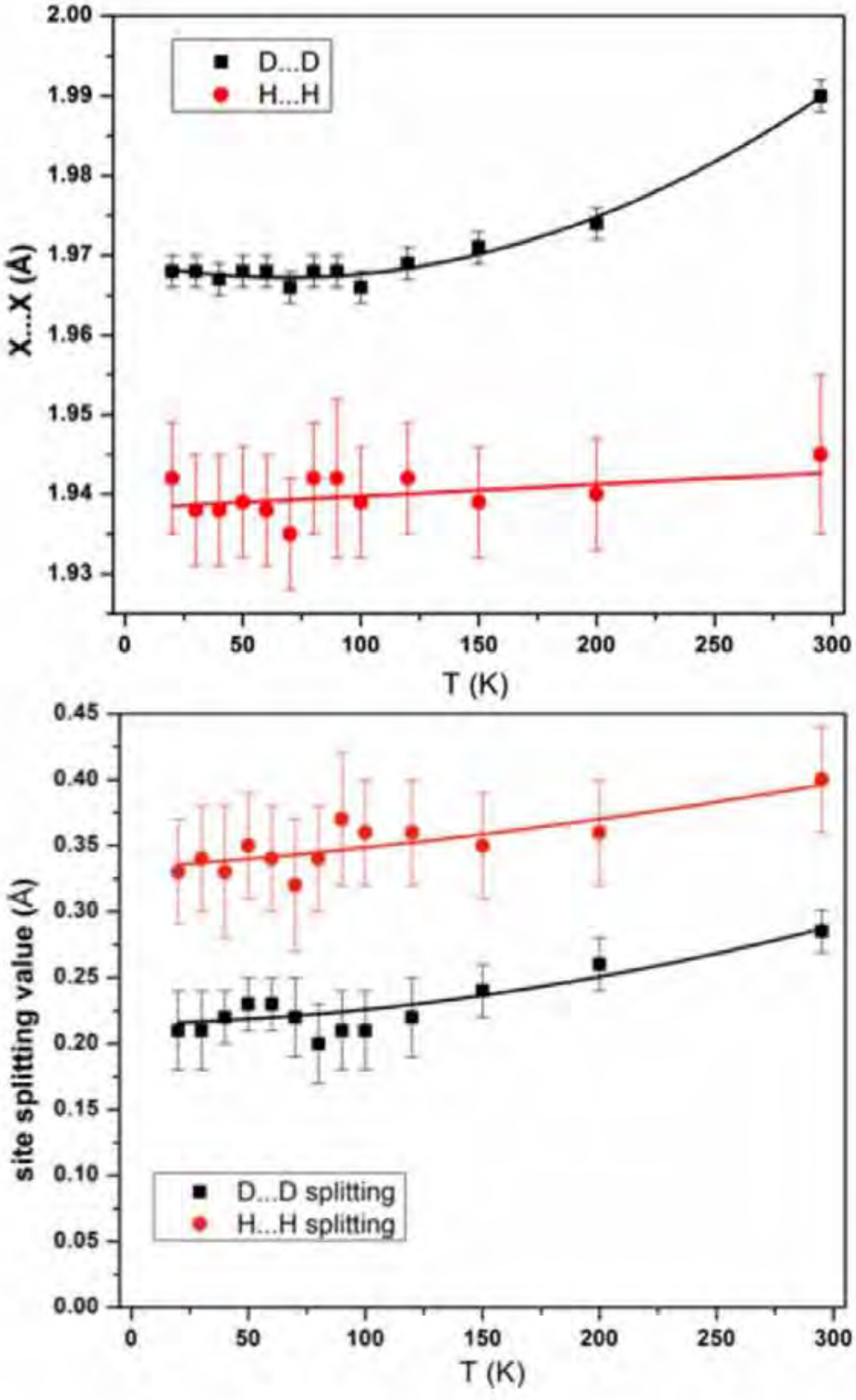
D...D
H...H
X...X (Å)
T (K)
D...D splitting
H...H splitting
site splitting value (Å)
T (K)

Fig 7

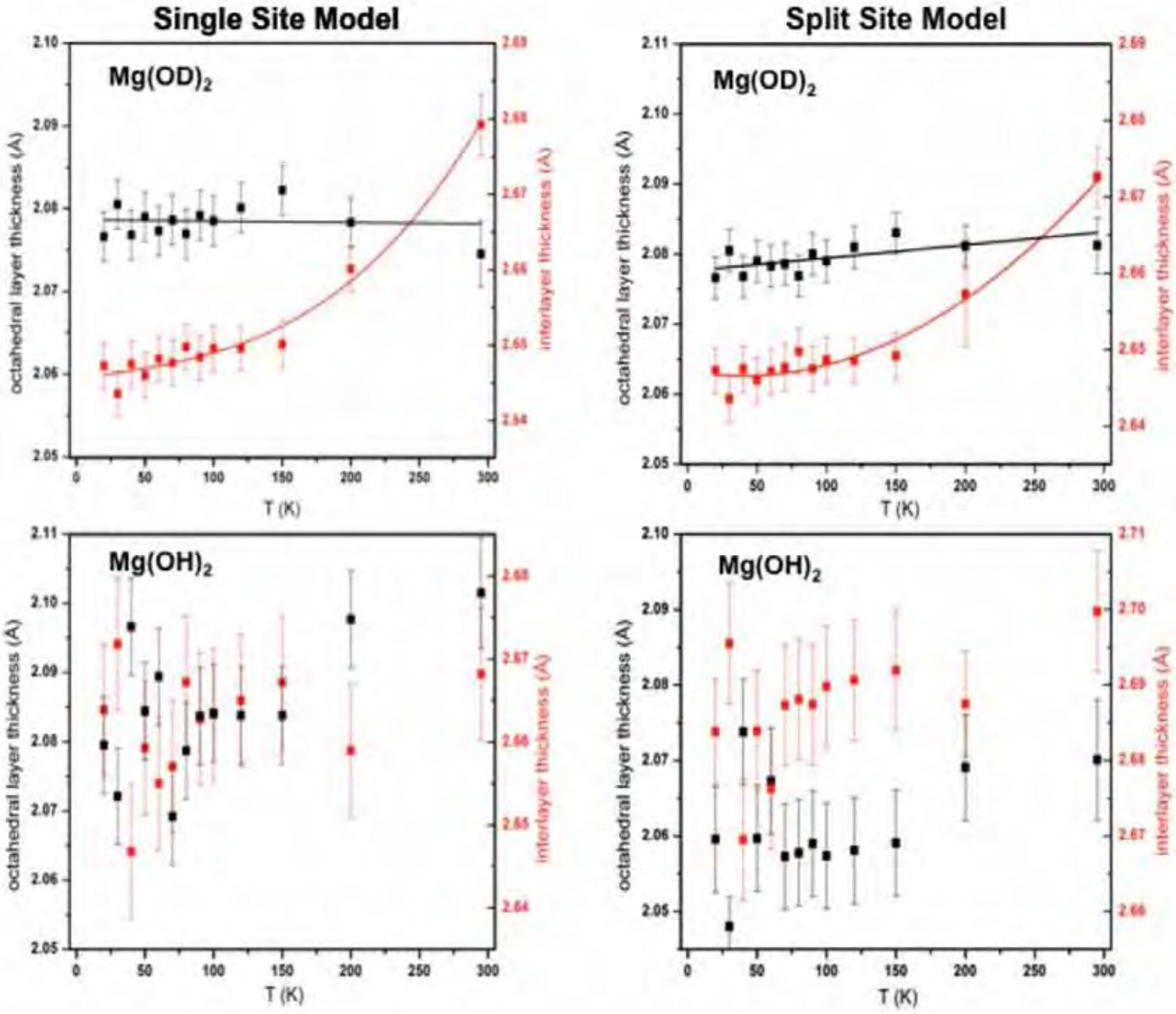
Single Site Model
Split Site Model
Mg(OD)2
Mg(OH)2
octahedral layer thickness (Å)
interlayer thickness (Å)
T (K)

Fig 8